Enhancement of specific absorption rate in lossy dielectric objects using a slab of left-handed material

Lei Zhao and Tie Jun Cui*

Center for Computational Electromagnetics and the State Key Laboratory of Millimeter Waves, Department of Radio Engineering, Southeast University, Nanjing 210096, People's Republic of China

(Received 20 August 2005; revised manuscript received 6 October 2005; published 19 December 2005)

An enhancement of the specific absorption rate (SAR) inside a lossy dielectric object has been investigated theoretically based on a slab of left-handed medium (LHM). In order to make an accurate analysis of SAR distribution, a proper Green's function involved in the LHM slab is proposed, from which an integral equation for the electric field inside the dielectric object is derived. Such an integral equation has been solved accurately and efficiently using the conjugate gradient method and the fast Fourier transform. We have made a lot of numerical experiments on the SAR distributions inside the dielectric object excited by a line source with and without the LHM slab. Numerical experiments show that SAR can be enhanced tremendously when the LHM slab is involved due to the proper usage of strong surface waves, which will be helpful in the potential biomedical applications for hyperthermia. The physical insight for such a phenomenon has also been discussed.

DOI: 10.1103/PhysRevE.72.061911 PACS number(s): 78.20.Ci, 87.54.Br, 41.20.Jb, 42.25.Bs

I. INTRODUCTION

In recent years, a lot of research has been conducted on the heating caused in a biological body by incident electromagnetic radiation [1–6]. Hyperthermia, the heating of a tumor to a temperature of 42–45 °C, has been an effective adjuvant for cancer therapy [7–9]. In order to obtain therapeutic temperatures in tumors and keep the temperatures in healthy tissues at acceptable levels, many heating techniques are employed at present using the electromagnetic waves and energies [8–10]. An important measure on hyperthermia for a biological object (or a lossy dielectric object) is a specific absorption rate (f_{SAR}, in W/kg), which is defined as

$$f_{\mathrm{SAR}} = \frac{1}{2}\frac{\sigma(\mathbf{r})}{\rho(\mathbf{r})}|E_y(\mathbf{r})|^2, \tag{1}$$

where σ is the conductivity of the dielectric object (in S/m), ρ is the density of the object (in kg/m^3), and $|E_y|$ is the magnitude of the electric field (in V/m). f_{SAR} describes the average power per unit mass of the object dissipated in heat.

There are many factors to influence the SAR distribution inside the dielectric body. A number of previous reports have studied the optimization technique in SAR distributions for electromagnetic hyperthermia using numerical and experimental methods [11–14]. However, most of the theoretical and experimental studies are focused on adjusting the phase of applicator arrays to change SAR distributions.

In this paper, we make use of the special physical characteristics of a left-handed medium (LHM) to control SAR distributions efficiently. The concept of LHM was proposed by Veselago in 1968 [15]. With negative permittivity and negative permeability simultaneously, LHM has been shown to possess a lot of exotic properties such as negative refraction, reversed Doppler shift, and reversed Cerenkov radiation. Moreover, a LHM slab can focus the incident waves and act as a lens [15]. However, not much attention has been paid to LHM due to the absence in nature until recently when the artificial LHM has been verified by experiments [16]. Periodic arrays of metallic rods and split ring resonators have been used to realize different materials [17,18]. Inspired by the experimental results, intensive studies have been conducted to understand the physical essences of the LHM.

One of the most attractive features of the LHM is the amplification of evanescent waves. Using such a feature, it has been shown that a lossless LHM slab can be made as a perfect lens [19]. Although the perfect lens has later been shown unphysical [20], a slightly lossy LHM slab is still able to be a superlens [21–24], where strong surface waves can be excited near the slab surfaces. In this paper, we will investigate the possibility to enhance the SAR distribution inside the lossy dielectric object using the LHM slab. Numerical experiments have shown that SAR can be controlled and enhanced tremendously due to the proper usage of the LHM slab.

II. GENERAL ANALYSIS

In order to seek the possibility of SAR enhancement, we have to compute the internal electric fields inside the lossy dielectric object accurately in a complicated environment. To this end, we consider a general problem involving a radiation source, a one-dimensional (1D) LHM slab, and an arbitrarily shaped dielectric object. For simplicity, we use a two-dimensional (2D) line source as the radiator and a 2D lossy dielectric cylinder as the target. As shown in Fig. 1, the line source and the dielectric object are located in regions 0 and 2 (free space), respectively, and region 1 is the LHM slab with the relative permittivity ϵ_{r1} and relative permeability μ_{r1}. Under the Cartesian coordinate shown in Fig. 1, the slab interfaces are located at $z=-d_2+d_1$ and $z=0$, and the line source is located at $(x,z)=(0,-d_2)$. According to Pendry's analysis, there is an interior image and an exterior image of the line source at points $(0,-d_2+2d_1)$ and $(0,d_2-2d_1)$, respectively.

*Email address: tjcui@seu.edu.cn

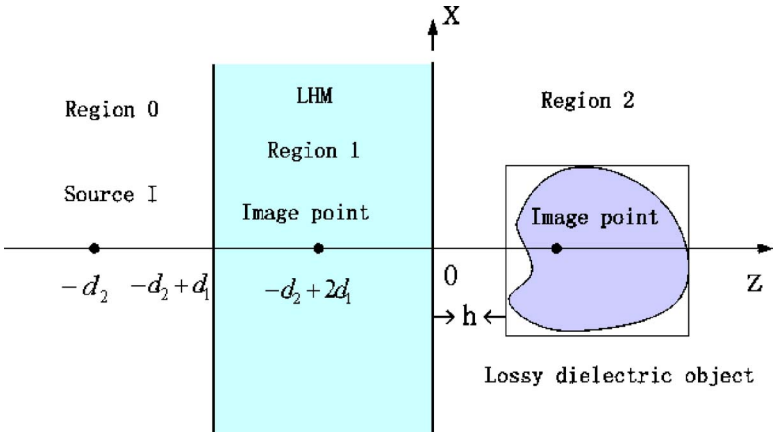

FIG. 1. (Color online) A general problem consisting of a line source, a 1D LHM slab, and a 2D lossy dielectric object. The source and object extend to infinity in the y direction, and the LHM slab extends to infinity in both x and y directions. The dielectric object can be arbitrarily shaped. The slab interfaces are located at $z=-d_2+d_1$ and $z=0$, and the line source is located at $(x,z)=(0,-d_2)$. There are two image points of the line source located at $(0,-d_2+2d_1)$ and $(0,d_2-2d_1)$, respectively.

As we know, the line source radiates a cylindrical wave expressed by the Hankel's function. When the 1D LHM slab exists, the cylindrical wave should be expanded as the integral summation of plane waves using the Wyle identity to get a closed-form solution [25]. After simple derivation, we obtain the electric field in region 2 radiated by the line source I as

$$E_{2y}^{inc}(x,z) = -\frac{\omega\mu_0}{4\pi} I \int_{-\infty}^{+\infty} dk_x \frac{1}{k_{0z}} T e^{ik_{2z}z} e^{ik_x x}, \tag{2}$$

which represents the incident field of the dielectric object. Here, T is the transmission coefficient of plane waves propagating along the positive z axis. From the boundary conditions, we have

$$T = \frac{4e^{ik_{0z}d_1}e^{ik_{1z}d}}{(1+P_{01})(1+P_{12})(1+R_{01}R_{12}e^{i2k_{1z}d})}, \tag{3}$$

in which $d=d_2-d_1$ is the slab thickness, $k_{iz}=\sqrt{k_i^2-k_y^2}$ $(i=0,1,2)$ is the propagating factor in region i, and

$$R_{01} = \frac{1-P_{01}}{1+P_{01}}, \quad R_{12} = \frac{1-P_{12}}{1+P_{12}} \tag{4}$$

are Fresnel reflection coefficients at slab interfaces, and

$$P_{01} = \frac{\mu_0 k_{1z}}{\mu_1 k_{0z}}, \quad P_{12} = \frac{\mu_1 k_{0z}}{\mu_0 k_{1z}}. \tag{5}$$

Under the excitation of the incident field $E_{2y}^{inc}(x,z)$, an equivalent volume current density will be produced inside the dielectric object, which is proportional to the internal electric field: $J_{2y}(x,z)=-i\omega\epsilon_0[\epsilon_r(x,z)-1]E_{2y}(x,z)+\sigma(x,z)E_{2y}(x,z)$. Here, $\epsilon_r(x,z)$ and $\sigma(x,z)$ are relative permittivity and conductivity of the lossy dielectric object. The radiation of such volume current results in a scattered electric field:

$$E_{2y}^{sca}(x,z) = k_0^2 \int_D dS' g(x-x',z,z') O(x',z') E_{2y}(x',z'), \tag{6}$$

where k_0 is the wave number of free space, $O(x,z)=\epsilon_r(x,z)-1+i\sigma(x,z)/(\omega\epsilon_0)$ is called an object function [26], and

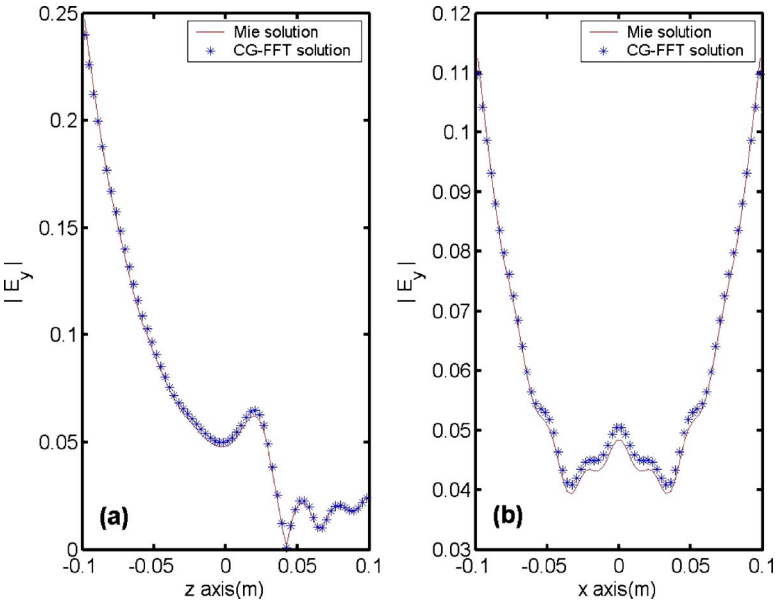

FIG. 2. (Color online) The electric-field distributions inside the homogeneous lossy circular cylinder in free space under the plane-wave excitation, where $\epsilon_r=50$, $\sigma=1.0$ S/m, and $\mu_r=1$ to simulate the human brain, and the working frequency is 900 MHz. Solid lines indicate the Mie series solutions and stars indicate the CG-FFT solutions. (a) Field values along the line $x=0$. (b) Field values along the line $z=0$.

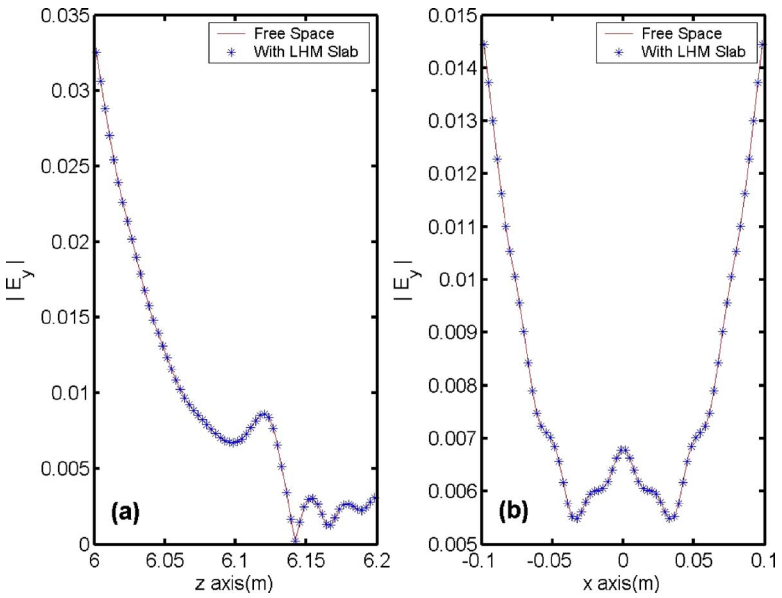

FIG. 3. (Color online) The electric-field distributions inside the homogeneous lossy circular cylinder with and without the LHM slab under the line-source excitation. Here, the object is far away from the slab ($h=6.0$ m), $\epsilon_r=50$, $\sigma=1.0$ S/m, $\mu_r=1$, and the working frequency is 900 MHz. Solid lines indicate the CG-FFT solutions in free space when the line source is placed at the exterior image point ($x=0$ and $z=0.2$ m) and stars indicate the CG-FFT solutions when the LHM slab exists and the line source is placed at $x=0$ and $z=-0.6$ m. (a) Field values along the line $x=0$. (b) Field values along the line $z=0$.

$g(x-x',z,z')$ is the Green's function involving the LHM slab.

In order to obtain the Green's function, we consider the radiation of a line source which is located at (x',z') in region 2. After a simple derivation [25,26], we obtain

$$g(x-x',z,z') = g_1(x-x',z-z') + g_2(x-x',z+z'), \quad (7)$$

in which

$$g_1(x-x',z-z') = \frac{i}{4}H_0^{(1)}(k_0|\mathbf{r}-\mathbf{r}'|) \quad (8)$$

is just the Green's function in free space, and

$$g_2(x-x',z+z') = \frac{i}{4\pi}\int_{-\infty}^{+\infty} dk_x \frac{1}{k_{0z}} \mathrm{Re}^{ik_{0z}(z+z')}e^{ik_x(x-x')} \quad (9)$$

describes the contribution of reflected field by the LHM slab. Here, R is the reflection coefficient of plane waves propagating along the negative z axis:

$$R = \frac{R_{01}+R_{12}e^{i2k_{1z}d}}{1+R_{01}R_{12}e^{i2k_{1z}d}}. \quad (10)$$

Based on the relation among the internal, scattered, and incident electric fields

$$E_{2y}(x,z) = E_{2y}^{inc}(x,z) + E_{2y}^{sca}(x,z), \quad (11)$$

we easily obtain an electric field integral equation for $E_{2y}(x,z)$ as

$$E_{2y}(x,z) - k_0^2\int_D dS' g(x-x',z,z')O(x',z')E_{2y}(x',z') = E_{2y}^{inc}(x,z). \quad (12)$$

Introducing equivalent volume current densities [26]

$$J_2(x,z) = O(x,z)E_{2y}(x,z), \quad (13)$$

$$J_2^{inc}(x,z) = O(x,z)E_{2y}^{inc}(x,z), \quad (14)$$

Eq. (12) is then simplified as

$$J_2(x,z) - k_0^2O(x,z)\int_D dS'[g_1(x-x',z-z') + g_2(x-x',z+z')]J_2(x',z') = J_2^{inc}(x,z). \quad (15)$$

Solving the above integral equation, the internal electric field $E_{2y}(x,z)$ will be determined through Eq. (13), and then the SAR distribution inside the dielectric object is obtained.

Generally, there are no analytical solutions to Eq. (15), and hence numerical methods have to be used. The method of moments (MOM) is a popular technique to convert the above integral equation into a matrix equation. However, the conventional MOM is very expensive, where the memory requirement is of $O(N^2)$ to store the matrix, and the numerical complexity is of $O(N^3)$ to solve the matrix equation, in which N is the number of pixels to divide the biological object.

From Eq. (15), however, we observe that the first term of the integral represents a 2D convolution and the second term represents a 1D convolution in x and 1D correlation in z. Hence such two terms can be performed rapidly using the fast Fourier transform (FFT). Actually, the conjugate gradient (CG) method with FFT is an efficient approach to solve the problem. For details, please refer to, for example, Refs. [26–28]. Using CG-FFT, the integral equation can be solved rapidly, where the memory requirement is only of $O(N)$, and the floating-point operations are only proportional to $C_1N_{iter}N\ln N$. Here, C_1 is a small constant and N_{iter} is the number of iterations.

III. NUMERICAL EXPERIMENTS

In this section, we explore the enhancement of SAR distributions inside the lossy dielectric object with the aid of the LHM slab through numerical experiments of two typical models. All numerical results are obtained by solving the

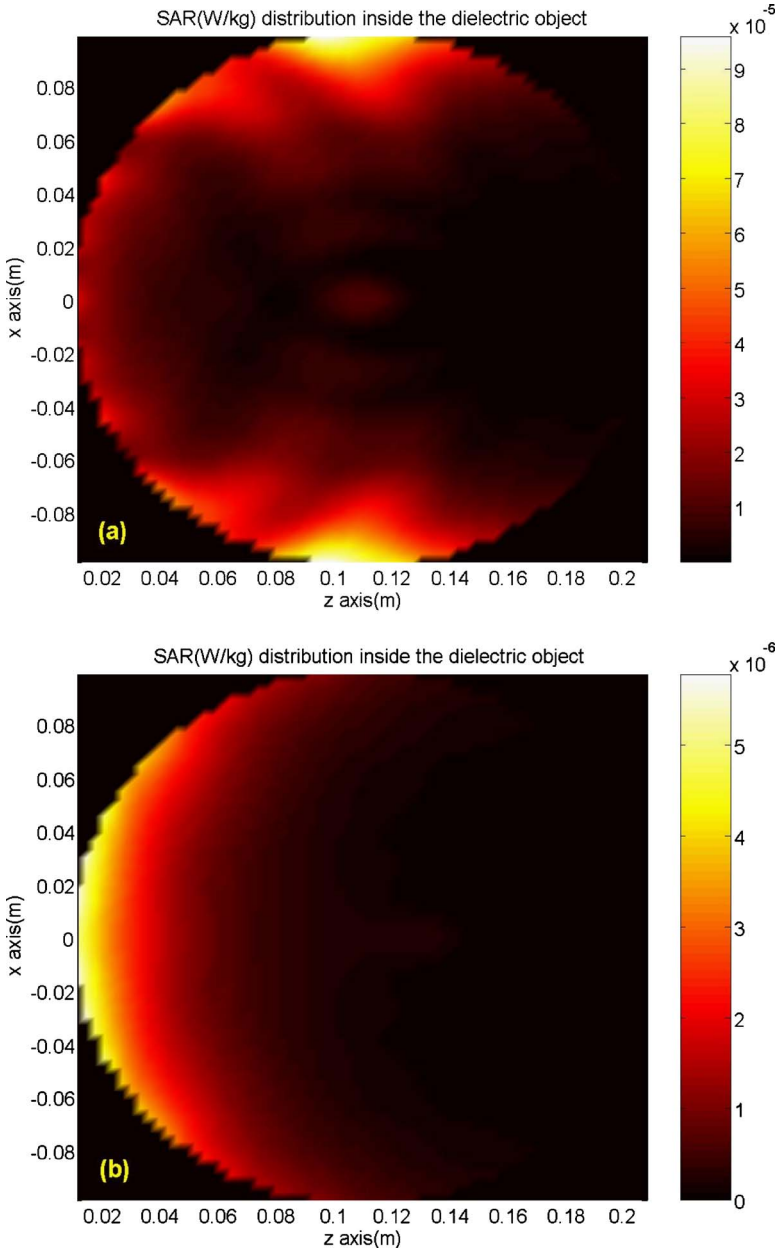

FIG. 4. (Color online) The SAR distribution inside the homogeneous lossy circular cylinder with and without the LHM slab under the line-source excitation when the object is very close to the slab ($h=0.01$ m). Here, $\epsilon_r=50$, $\sigma=1.0$ S/m, $\mu_r=1$, and the working frequency is 900 MHz. (a) With the LHM slab. (b) Without the LHM slab.

integral equation (15) using the CG-FFT method. The line source with the electric current of 1 mA is located at the point $x=0$ and $z=-0.6$ m. The LHM slab is characterized as $\epsilon_{r1}=-1+10^{-4}+i10^{-6}$ and $\mu_{r1}=-1+10^{-4}+i10^{-6}$, whose boundaries reside at $z=-0.4$ m and $z=0$, respectively.

A. A homogeneous circular cylindrical model

We first adopt a simple model of homogeneous circular cylinder, which has a diameter of 0.2 m. The corresponding physical parameters are $\epsilon_r=50$, $\sigma=1.0$ S/m, $\mu_r=1$, and $\rho=1$ g/cm^3 to simulate the human brain. In this example, the working frequency is 900 MHz.

In order to verify the accuracy of the field distributions computed by the CG-FFT method, we first consider a simple case of plane-wave incidence to the lossy circular cylinder in free space, where an exact solution exists using the Mie series. Figure 2 illustrates the comparison of internal electric fields along the lines $x=0$ and $z=0$, respectively. From Fig. 2, we clearly see that the numerical results computed from CG-FFT have excellent agreement with the exact values. Since the plane-wave excitation only appears in the right-hand side (RHS) of Eq. (15), the above conclusion can be easily extended to the line-source case by replacing the RHS with the line-source excitation.

In the earlier example, the excellent agreements have validated the accuracy of the numerical method for the free-space kernel $g_1(x-x',z-z')$. To validate the LHM kernel $g_2(x-x',z,z')$ furthermore, we compute the electric fields inside the dielectric object under the excitation of the line source. When the LHM slab exists and the dielectric object is far away from the slab ($h=6.0$ m), the internal electric fields along the lines $x=0$ and $z=0$ are demonstrated in Fig. 3 (stars).

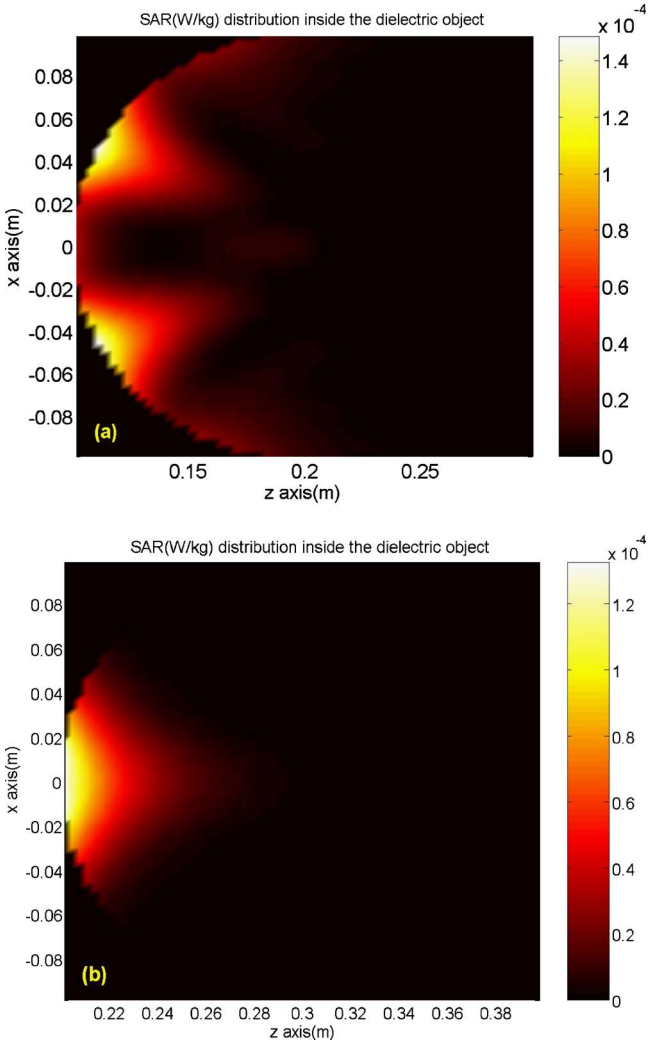

FIG. 5. (Color online) The SAR distributions inside the homogeneous lossy circular cylinder with the LHM slab under the line-source excitation for different distances h. Here, $\epsilon_r=50$, $\sigma=1.0$ S/m, $\mu_r=1$, and the working frequency is 900 MHz. (a) $h=0.1$ m. (b) $h=0.2$ m.

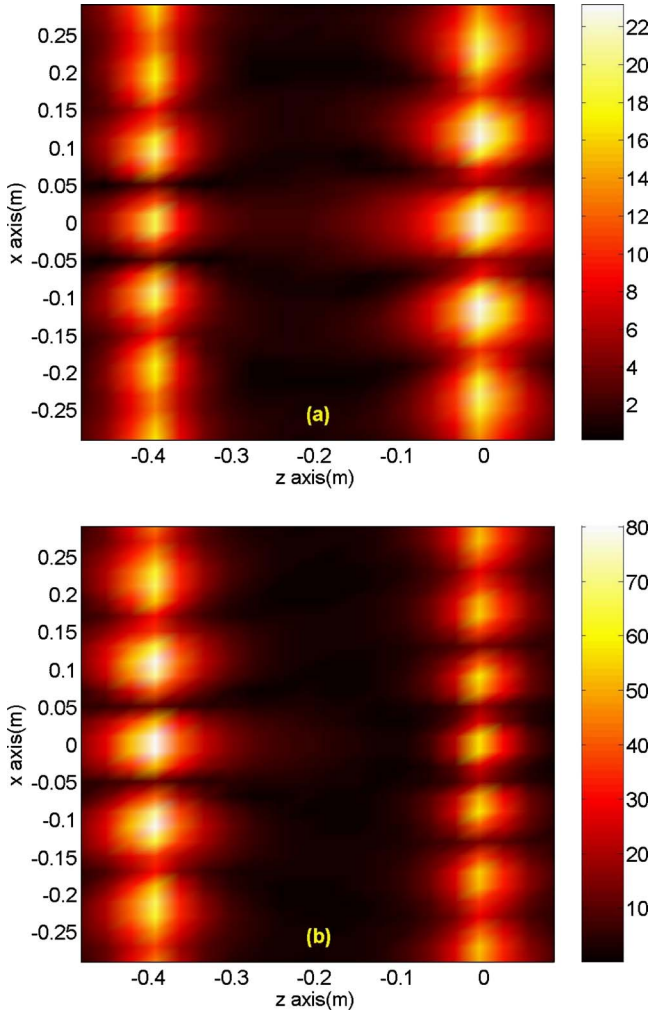

FIG. 6. (Color online) The electric-field distributions inside and outside the LHM slab under the line-source excitation, where the working frequency is 900 MHz. (a) The circular dielectric object does not exist, where strong surface waves are observed on the slab boundaries. (b) The circular dielectric object exists, where $\epsilon_r=50$, $\sigma=1.0$ S/m, $\mu_r=1$, and $h=0.1$ m. Clearly, both the amplitude and pattern of surface waves have been changed due to the effect of strong volume currents inside the dielectric object.

As we know, one important feature of the LHM slab is the superlens [19]. Under the chosen parameters ($\epsilon_{r1}=-1+10^{-4}+i10^{-6}$ and $\mu_{r1}=-1+10^{-4}+i10^{-6}$), nearly all propagating waves emitted from the line source I will be recovered at the image points, and most of evanescent waves will be amplified. When the biological object is far away from the source, only the propagating waves play important roles in the internal electric fields because evanescent waves decay to very small values. As a consequence, if we remove the LHM slab and put the line source at the exterior image point ($x=0$ and $z=0.2$ m), the computed electric fields will be nearly the same as those mentioned earlier. Figure 3 (solid lines) illustrates such numerical results. The excellent agreements between such two results (stars and solid lines) validate the accuracy of the CG-FFT method with the LHM kernel.

Now we investigate the SAR distributions inside the lossy dielectric object. When the LHM slab exists and the object is very close to the slab ($h=0.01$ m), the SAR distributions computed by CG-FFT are demonstrated in Fig. 4(a). To view the effect of the LHM slab, the SAR distributions are also computed without the LHM slab, as shown in Fig. 4(b).

Comparing Figs. 4(a) with 4(b), we clearly see that SAR inside the lossy dielectric object has been enhanced by a factor of 16 with the use of LHM slab. From Fig. 4(b), we also notice that the SAR distribution is strong close to the source and weak far from the source if we remove the LHM slab. With the LHM slab, however, the SAR pattern has been changed tremendously, where the strong SAR regions appear in two small parts in the top and bottom, as shown in Fig. 4(a).

If we increase the distance between the circular dielectric object and the slab, we can further change the SAR patterns. Figure 5 illustrates the SAR distributions inside the dielectric object when $h=0.1$ m and $h=0.2$ m, respectively. From Fig. 5(a), the two strong SAR spots move to the front region of the cylinder in the case of $h=0.1$ m. When h increases to 0.2

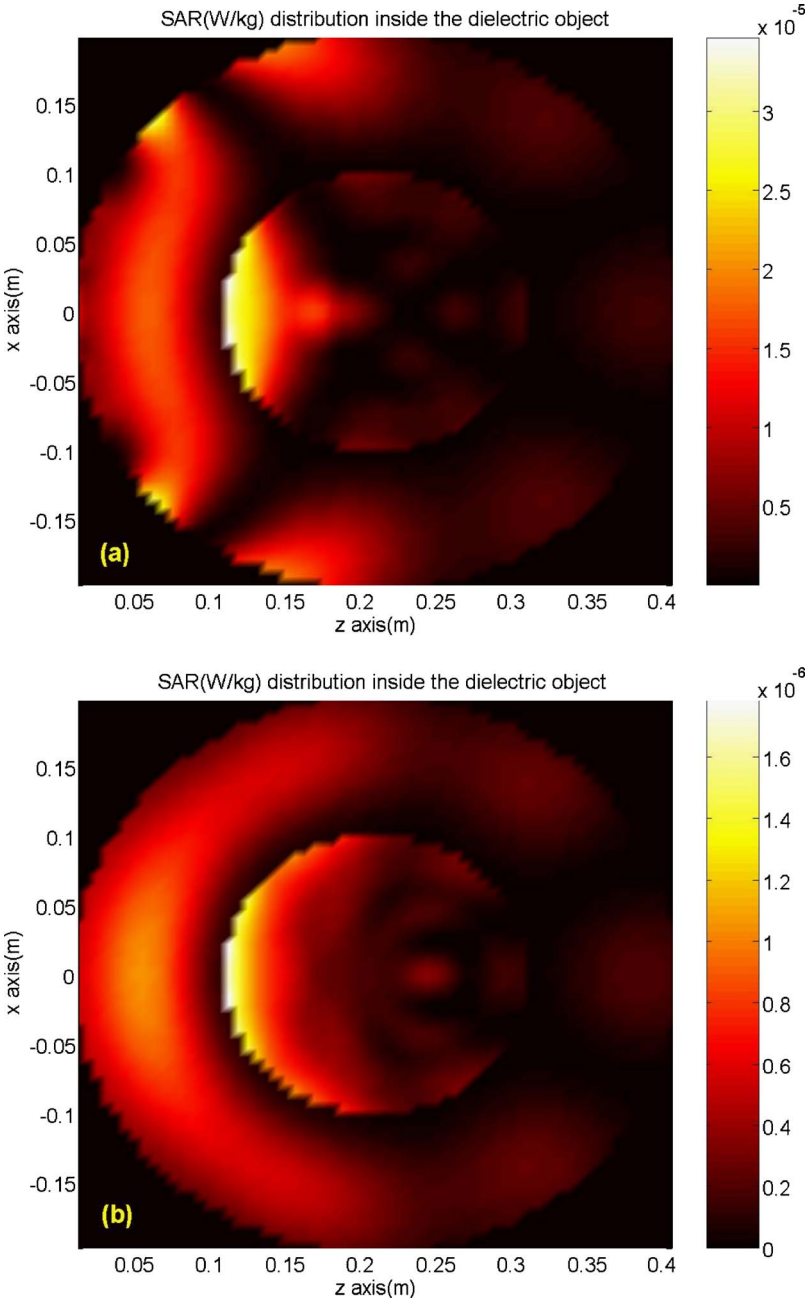

FIG. 7. (Color online) The SAR distributions inside the two-layered lossy circular dielectric cylinder with and without the LHM slab under the line-source excitation when the object is very close to the slab (h=0.01 m). Here, the outer layer has a diameter of 0.4 m to simulate fat, whose physical parameters are ϵ_r=7.5, σ =0.048 S/m, and ρ=0.9 g/cm^3; the inner layer has a diameter of 0.2 m to simulate muscle, whose physical parameters are ϵ_r=72, σ =0.9 S/m, and ρ=1.02 g/cm^3; the working frequency is 500 MHz. (a) With the LHM slab. (b) Without the LHM slab.

m, the two SAR hot spots merge to one, appearing in the front region, as shown in Fig. 5(b). If the LHM slab does not exist, however, the SAR patterns are nearly unchanged in moving the biological object from h=0.01 m to h=0.2 m.

The physical reason to enhance SAR and to change the SAR patterns is the proper usage of surface waves around the LHM slab. As we know, strong surface waves are generated on the two slab boundaries under the excitation of a line source. Figure 6(a) illustrates the electric-field distributions inside and outside the LHM slab when the dielectric object does not exist, where strong surface waves are clearly observed. Such strong surface waves will then produce strong internal electric fields inside the dielectric object which is close to the slab to enhance SAR. Actually, the strong surface waves on the slab boundaries can be regarded as an array of sources with different phases, which results in the change of SAR patterns when we move the biological body, as shown in Figs. 4 and 5.

On the other hand, the large internal electric fields inside the lossy dielectric object (or the equivalent volume currents) will affect the surface-wave distributions. Figure 6(b) demonstrates the electric fields inside and outside the LHM slab when the dielectric object exists, where h=0.1 m. Comparing Figs. 6(a) and 6(b), we clearly observe that the amplitude of surface waves has been increased tremendously due to the existence of the dielectric object and the wave pattern has also been changed.

B. A two-layered circular cylindrical model

Next we consider a two-layered circular cylindrical structure to model the human tissue. Here, the outer layer has a

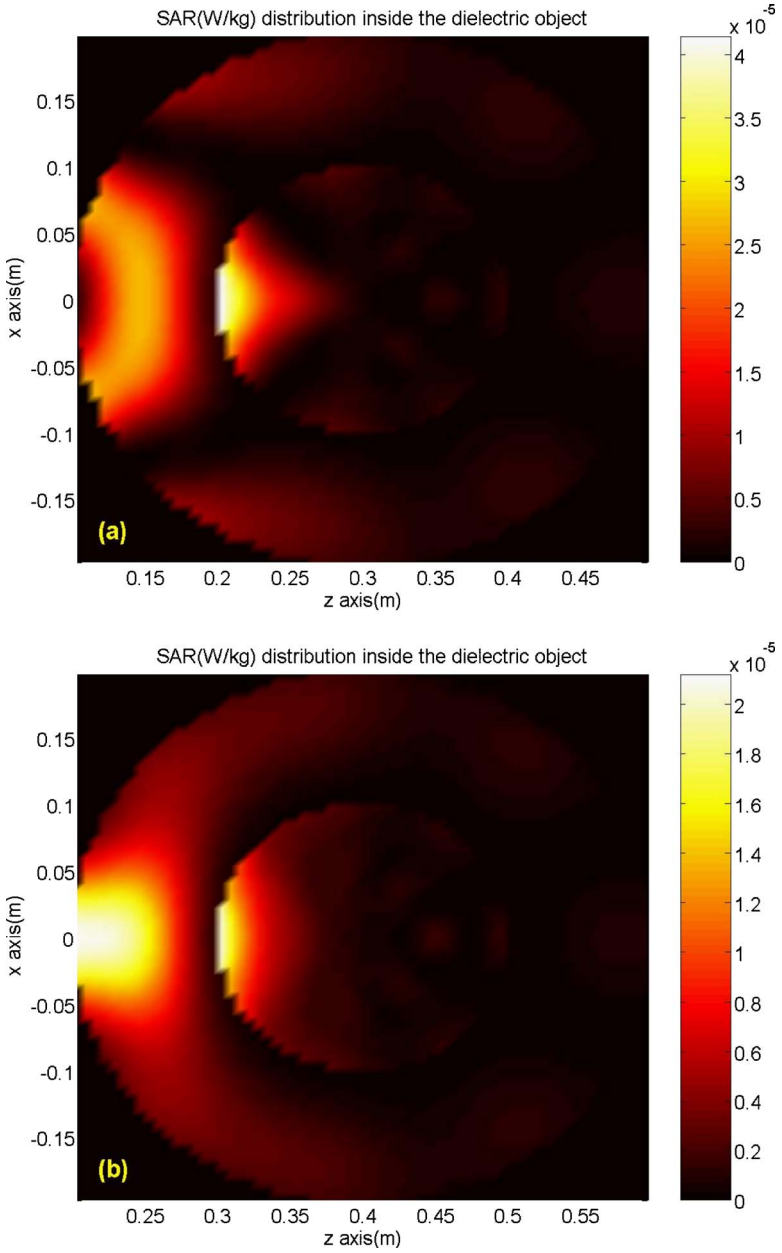

FIG. 8. (Color online) The SAR distributions inside the two-layered lossy circular dielectric cylinder with the LHM slab under the line-source excitation for different distances h. Here, the object parameters are the same as those in Fig. 7 and the working frequency is 500 MHz. (a) $h=0.1$ m. (b) $h=0.2$ m.

diameter of 0.4 m to simulate fat, whose physical parameters are $\epsilon_r=7.5$, $\sigma=0.048$ S/m, and $\rho=0.9$ g/cm^3. The inner layer has a diameter of 0.2 m to simulate muscle, whose physical parameters are $\epsilon_r=72$, $\sigma=0.9$ S/m, and $\rho=1.02$ g/cm^3. The same source and LHM slab have been used and the working frequency is 500 MHz in this case.

When the two-layered dielectric object is close to the LHM slab ($h=0.01$ m), the computed SAR distribution inside the object is illustrated in Fig. 7(a). Again, we also give the SAR distribution if the LHM slab does not exist for easy comparison, as shown in Fig. 7(b). From Fig. 7, it is evident that SAR inside the two-layered dielectric object is enhanced by a factor of 21 with the aid of LHM slab. On the other hand, the SAR pattern has been changed and the strong SAR region is more focused. By adjusting the distance h between the object and slab, the strong SAR parts can be changed due to the strong surface waves around the LHM slab, as shown in Fig. 8.

Therefore the LHM slab can play a very important role in the SAR enhancement and the control of SAR patterns. By adjusting the distance between the lossy dielectric object and slab, we can properly make use of the strong surface waves around the slab. Then the SAR distribution will be greatly enhanced. In the meantime time, the strong SAR parts can be focused to certain small areas due to the array effect of surface waves, which will be helpful in the potential biomedical applications, such as the hyperthermia for cancer therapy.

IV. CONCLUSIONS

We have proposed an efficient technique to enhance the SAR distributions in lossy dielectric objects and adjust the focus points using the LHM slab. An accurate method has been developed to investigate the above features through numerical experiments, where a proper Green's function in-

volved in the LHM slab is given and the resulting integral equation has been solved numerically using the CG-FFT technique. Numerical experiments show that the LHM slab plays a important role in the SAR enhancement and the change of SAR patterns. When we adjust the distance between the biological object and the LHM slab, the strong surface waves around the LHM slab can be properly used to enhance the SAR distribution. Moreover, the strong SAR regions can be focused to certain small areas, which will be very helpful in hyperthermia for cancer therapy.

ACKNOWLEDGMENTS

This work was supported in part by the National Basic Research Program (973) of China under Grant No. 2004CB719800, in part by the National Science Foundation of China for Distinguished Young Scholars under Grant No. 60225001, in part by the National Science Foundation of China under Grant No. 60496317, and in part by the National Doctoral Foundation of China under Grant No. 20040286010.

[1] M. Okoniewski and M. A. Struchly, IEEE Trans. Microwave Theory Tech. **44**, 1855 (1996).
[2] V. Hombach, K. Meier, M. Burkhardt, E. Kühn, and N. Kuster, IEEE Trans. Microwave Theory Tech. **44**, 1865 (1996).
[3] Q. P. Gandhi and J. Y. Chen, IEEE Trans. Electromagn. Compat. **37**, 547 (1995).
[4] R. W. P. King, Radio Sci. **30**, 267 (1995).
[5] L. Martens, J. De Moerloose, D. De Zutter, J. De Poorter, and C. De Wagter, Radio Sci. **30**, 283 (1995).
[6] J. De Poorter, and V. Hombach, IEEE Trans. Electromagn. Compat. **40**, 547 (1998).
[7] J. L. Meyer, Cancer Res. **44**, 4745 (1984).
[8] *Physical Techniques in Clinical Hyperthermia*, edited by J. W. Hand and J. R. James (Research Studies Press, Latchworth, U. K., 1986).
[9] O. S. Nielsen, M. Horsman, and J. Overgaard, Eur. J. Cancer **37**, 1587 (2001).
[10] N. Siauve, L. Nicolas, C. Vollaire, A. Nicolas, and J. A. Vasconcelos, IEEE Trans. Microwave Theory Tech. **40**, 1264 (2004).
[11] C. De Wagter, IEEE Trans. Microwave Theory Tech. **34**, 589 (1986).
[12] F. Jouvie, J. C. Bolomey, and G. Gaboriaud, IEEE Trans. Microwave Theory Tech. **34**, 495 (1986).
[13] J. W. Strohbehn, E. H. Curtis, K. K. Paulsen, X. Yuan, and D. R. Lynch, Int. J. Radiat. Oncol., Biol., Phys. **16**, 589 (1989).
[14] G. Arcangeli, P. P. Lombardini, G. A. Lovisolo, G. Marsiglia, and M. Piattelli, IEEE Trans. Biomed. Eng. **31**, 47 (1984).
[15] V. G. Veselago, Usp. Fiz. Nauk **92**, 517 (1967) [Sov. Phys. Usp. **10**, 509 (1968)].
[16] R. A. Shelby, D. R. Smith and S. Schultz, Science **292**, 77 (2001).
[17] J. B. Pendry, A. J. Holden, W. J. Stewart, and I. Youngs, Phys. Rev. Lett. **76**, 4773 (1996).
[18] D. R. Smith, W. J. Padilla, D. C. Vier, S. C. Nemat-Nasser, and S. Schultz, Phys. Rev. Lett. **84**, 4184 (2000).
[19] J. B. Pendry, Phys. Rev. Lett. **85**, 3966 (2000).
[20] N. Garcia and M. Nieto-Vesperinas, Phys. Rev. Lett. **88**, 207403 (2002).
[21] T. J. Cui, Z. C. Hao, X. X. Yin, W. Hong, and J. A. Kong, Phys. Lett. A **323**, 484 (2004).
[22] D. R. Smith, D. Schurig, M. Rosenbluth, S. Schultz, S. A. Ramakrishna, and J. B. Pendry, Appl. Phys. Lett. **82**, 1506 (2003).
[23] T. J. Cui, Q. Cheng, W. B. Lu, Q. Jiang, and J. A. Kong, Phys. Rev. B **71**, 045114 (2005).
[24] Q. Cheng, T. J. Cui, and W. B. Lu, Phys. Lett. A **336**, 235 (2005).
[25] W. C. Chew, *Waves and Fields in Inhomogenous Media* (Van Nostrand Reinhold, New York, 1990).
[26] T. J. Cui, W. C. Chew, A. A. Aydiner, and S. Y. Chen, IEEE Trans. Geosci. Remote Sens. **39**, 339 (2001).
[27] M. F. Catedra, E. Gago, and L. Nuno, IEEE Trans. Antennas Propag. **37**, 528 (1989).
[28] T. J. Cui and W. C. Chew, IEEE Trans. Geosci. Remote Sens. **37**, 2597 (1999).